Simultaneous optical and X-ray high speed photometry of Cyg X-2

G. Dubus[1]⋆, B. Kern[2], A. A. Esin[3], R. E. Rutledge[1] and C. Martin[2].

[1] *California Institute of Technology, MC 130-33, Pasadena, CA 91107*
[2] *California Institute of Technology, MC 405-47, Pasadena, CA 91107*
[3] *Harvey Mudd College, 301 E. 12th Street, Claremont, CA 91711*

ABSTRACT

The X-ray emission from X-ray binaries may originate in flares occurring when magnetic loops anchored in the disc reconnect. In analogy with our Sun, Hα emission should arise as the accelerated electrons thermalize in the optically emitting disc, perhaps leading to correlated variability between X-rays, Hα and the optical continuum. We present simultaneous X-ray and optical high speed photometry of the neutron star low-mass X-ray binary Cyg X-2 to search for such correlations. The highest time resolution achieved is 5 ms in white light and 100 ms with a 3 nm filter centred on Hα. We find power on timescales $\gtrsim$ 100s (flickering) in optical with a total r.m.s. of a few %, about an order of magnitude less than that seen in X-rays. We do not find significant correlations between the X-ray and optical fluxes on short timescales, hence cannot conclude whether magnetic flares contribute significantly to the optical emission.

Key words: accretion, accretion discs — binaries: close — stars: individual (V1341 Cyg) — X-rays: individual (Cyg X-2)

1 INTRODUCTION

Observations of low mass X-ray binaries (LMXBs) show that strong emission at X-ray energies $\lesssim$ 100 keV is nearly ubiquitous in these systems (e.g. Done 2002). The standard optically thick, geometrically thin accretion disc (Shakura & Sunyaev 1973) cannot explain X-ray emission beyond a few keV. Thus, the observed hard X-rays as well as strong evidence for extended "coronal" emission in eclipsing LMXBs (van Paradijs & McClintock 1995) require more elaborate accretion flow models. A popular scenario, inspired by the solar corona, suggests that the cool Shakura & Sunyaev disc is sandwiched between two layers of hot plasma heated by reconnection of magnetic field loops anchored in the disc (Galeev, Rosner & Vaiana 1979; Haardt & Maraschi 1991). The presence of such a magnetically-heated corona would not be surprising, considering that angular momentum in discs is most likely transported outwards by turbulent magnetic stresses (Balbus & Hawley 1998). In the context of this model the observed X-ray spectra are interpreted as time-averaged emission from multiple coronal flares, while the characteristic X-ray time variability seen both in neutron star and

black hole systems (*e.g.,* van der Klis 2000) is then related to a distribution of flare strengths and durations.

In our Sun, bursts of hard X-ray emission from coronal flares are accompanied by simultaneous Hα line emission when the beam of electrons accelerated during reconnection is thermalised in the photosphere (*e.g.,* Dulk 1985). If the origin of X-ray emission is similar to that in solar flares, correlations between Hα and X-ray emission should occur on timescales ranging from the rise time of the flares ($\sim$ 0.01s) to their life time (either the dynamical time of the accretion disc at the radius where a flare occurs, or the thermal time needed to dissipate the energy of the wound-up magnetic field, up to $\sim$ tens of seconds at the outer edge of the disc). In the optical spectra of LMXBs, Hα is the strongest line (EW $\sim$ 1–10 Å, FWHM $\sim$ 1000–3000 km s^{-1}) and its double-peaked emission profile is an unambiguous signature of the accretion disc (van Paradijs & McClintock 1995). The disc is optically thick, so the line has to be produced in a thermally inverted layer, presumably located above the photosphere. However, if we pursue the analogy with the Sun, the heating source of this disc chromosphere, be it coronal flares, viscosity, reprocessing of X-rays or MHD waves, has yet to be understood.

A significant fraction of the optical flux in persistent LMXBs comes from the reprocessing in the disc of high energy photons produced in the inner parts of the accretion disk, or in the NS boundary layer

⋆ Present address: Laboratoire Leprince-Ringuet, CNRS/IN2P3, Ecole Polytechnique, F-91128, Palaiseau, France

(van Paradijs & McClintock 1995; O'Brien et al. 2002). This effect is most clearly demonstrated by the optical echoes of NS X-ray bursts observed in some systems. A few second delay between these optical echos and the X-ray bursts is interpreted as the light travel time to the reprocessing site (*e.g.,* O'Brien et al. 2002). This delayed heating of the disk by non-local radiation can in principle be distinguished from quasi-instantaneous local heating by particles accelerated in flares using high time resolution simultaneous X-ray and optical observations.

While the X-ray timing properties of LMXBs are well established, little is known about short-timescale non-orbital variations in the optical. On timescales $\gtrsim 1$ min flickering in white light (characterised by erratic flux changes by factors $\lesssim 2$) is a common occurrence in both persistent and transient LMXBs. The NS LMXB Sco X-1 shows intermittent correlated X-ray/optical flares related to non-local reprocessing (Ilovaisky et al. 1980; Petro et al. 1981). LMC X-2 also displays similar behaviour (McGowan et al. 2003). Recent monitoring of low-luminosity black hole LMXBs has revealed intriguing optical flares on timescales of tens of seconds (Hynes et al. 2003b). On the other hand, on timescales $\lesssim 1$ min, the variability of the optical continuum or Hα emission in LMXBs and its correlation with X-rays are still largely unexplored; such studies are hampered by the faintness of most systems, even when in outburst. Only two LMXBs have well established X-ray/optical continuum correlated behaviour on very short timescales (down to a few ms): GX 339-44 (Motch et al. 1983) and XTE J1118+480 (Kanbach et al. 2001; Hynes et al. 2003a). In both the variable optical flux has been interpreted as synchrotron emission from energetic flares (Fabian et al. 1982; di Matteo, Celotti & Fabian 1997).

In this paper we report on simultaneous X-ray and Hα/white light high time resolution observations of Cyg X-2, an optically bright ($V \sim 14.8$) persistent LMXB with a neutron star primary (*e.g.,* Orosz & Kuulkers 1999). Cyg X-2 has rapid (hour–days) X-ray spectral variations closely related to the timing properties: the slope/amplitude of the power law and the frequency of quasi-periodic oscillations (QPOs, $\nu \sim$1-20 Hz) seen in the power spectrum vary with the X-ray colours (*e.g.,* Wijnands et al. 1997). The optical flux varies by $\lesssim 1$ mag on timescale of hours to days, and flickering is reported in the brightest state. An ellipsoidal modulation on the orbital period of 9.8 days is observed with a V band amplitude of 0.1 mag. The donor star contributes about 50–70% of the total optical flux. Hα is known to vary on timescales of hours to days (see §4), but no systematic study of the Hα line variability has ever been undertaken. Here, we describe our search for correlated rapid variations between the X-ray and optical fluxes of Cyg X-2.

2 OBSERVATIONS AND DATA REDUCTION

We studied the variability of the optical continuum, Hα line emission and X-ray flux of Cyg X-2 at frequencies $\lesssim 100$ Hz using simultaneous data obtained on 2–4 August 2001 (UT) at the Hale 200-inch at Palomar and with the *Rossi X-ray Timing Explorer* (*RXTE*).

2.1 X-ray data

Cyg X-2 was observed with *RXTE/PCA* (Swank et al. 1996) on three consecutive nights (2–4 Aug 2001), for three consecutive orbits on each night. Data were analysed using FTOOLS v5.0. For all nine separate observations, we used data types collected by the Experiment Data System (EDS) in three modes (`SB_125us_0_13_1s`, `SB_125us_14_17_1s`, `SB_125us_18_23_1s`), which collected counts of 2.0-5.7 keV (centroid energies), 6.1-7.4 keV, and 7.8-9.8 keV. We made use of event mode data (`E_125_64M_24_1s`) in the 9.5-20 keV energy range. The time-tags associated with the counts were corrected to the solar-system barycenter in the DE405 time system using `axbary`.

We extracted a spectrum from the Standard 2 EDS mode data from the first night's observation. Examination of this spectrum showed that the countrate in excess of the background by a factor of 2-3 orders of magnitude up to 10 keV, and by a factor of 2-10 in the 10-20 keV energy range. We neglected the background for the spectral analyses herein. The 2.0-9.8 keV lightcurves (rebinned on 32 s from the original resolution of 1/256s) for each of the 9 visits are shown in the bottom panel of Fig. 1. The dip in countrate during the third visit is typical of the flaring branch (see §3.1).

2.2 Optical data

High-speed optical photometry of Cyg X-2 was obtained using a CCD in a multiple frame-transfer observing mode. The detector used is a SITe SI-502A thinned, AR-coated, back-illuminated 512×512-pixel CCD. The F/9 Cassegrain focus of the Palomar 200-inch telescope illuminated a 200×4 arcsec slit, which was re-imaged onto the uppermost rows of the CCD. The image was demagnified to a plate scale of 0.4 arcsec/pixel, yielding a slit size of 500×10 pixels. The un-illuminated portion of the CCD was used as storage, allowing 50 images to be accumulated before reading out the entire CCD. The transfer time, the time required to shift an image from the illuminated region of the CCD into storage, is short, so the shutter remained open during the accumulation of all 50 images, and was only closed during readout.

The timing of the images in a single frame was controlled by a GPS receiver and time-code generator. The GPS timing allowed control of the start time (and duration) of each image to an accuracy of 1 μs. The transfer time is 420 μs (42 μs per row shift), which occurs immediately following the start of a given image. The effective exposure time is the same for every image on the CCD except for the first and last few images. The first image or images have an effective exposure time that is reduced by the time it takes the shutter to open, which is approximately 13 ms. The last image has an effective exposure time that is increased by the time it takes the shutter to close, although the readout takes place during this time, resulting in some smearing. For this reason, the first image or images and the last image are discarded in the photometric analysis.

CCD pixels can be digitized in 22.4 μs, or discarded in 2.4 μs. To minimize the time spent reading the CCD, two windows are defined, which mark ranges of columns in which the pixels are digitized, with pixels in all other columns discarded. Each window was 40 pixels wide, which allowed the

Table 1. Log of Cyg X-2 Optical Observations.

Date 2001	Band	Δt ms	start	stop	Aper pixels	S/N	samples per frame	# frames	samples kept
Aug, 2	wl	5	4.107	4.943	7×7	17.2	47	1200	56237
Aug, 2	Hα	100	5.842	8.173	3×3	5.3	48	1100	52573
Aug, 3	Hα	100	29.490	30.325	3×3	4.3	48	400	19164
Aug, 3	wl	10	30.970	34.801	7×7	10.5	47	4400	113572
Aug, 4	wl	5	53.211	54.193	7×7	16.5	46	1200	50484
Aug, 4	Hα	100	54.759	58.980	3×3	4.6	48	2000	63041

Hα refers to a 3 nm filter centred on 656.2 nm, *wl* refers to observations taken in white light; Δt is the time resolution of the data; start and stop times are in hours from MJD 52123.0 UT ; Aper. is the size of the (square) aperture used for photometry in pixels; S/N is the observed signal-to-noise of each Δt exposure; samples per frame is the number of exposures on each CCD frame; last column is the number of flux measurements kept after bad data points were removed (see §2.2).
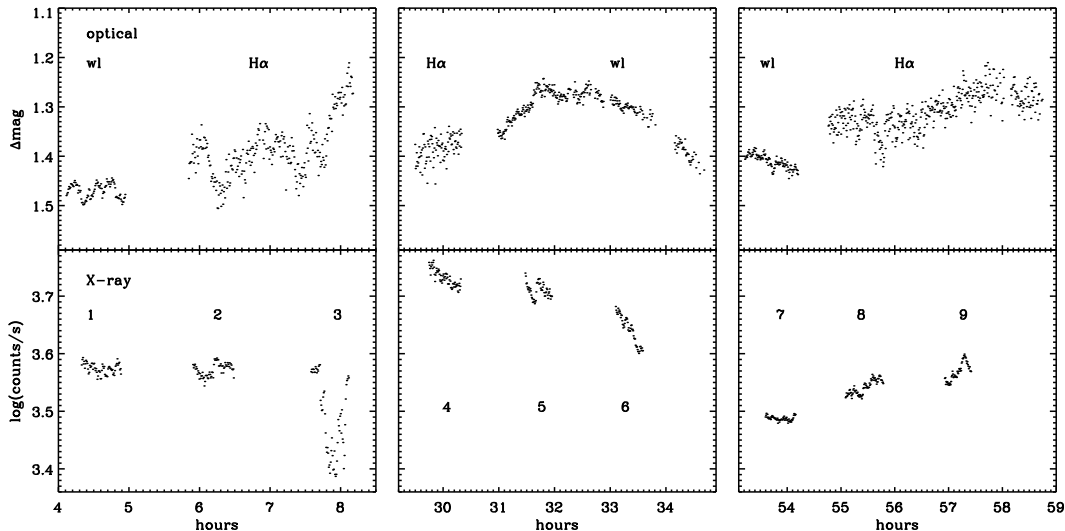

Figure 1. Simultaneous optical (top, Palomar 200-inch) and X-ray (bottom, *RXTE*) lightcurves of Cyg X-2. The time is in hours from MJD 52123. Each point is a 32 s (elapsed time) average. The type of photometry (white light or Hα filter) is indicated above each optical lightcurve. Δmag is the differential magnitude between Cyg X-2 and the comparison star. The X-ray count rate was derived from PCA channels 0–23 (2.0–9.8 keV). Cyg X-2 was on the normal branch during the first two X-ray visits, on the flaring branch on the third and on the horizontal branch in the subsequent observations. Typical error bars for the 32 s photometry bins are 0.002-0.003 mag in white light, 0.014-0.018 mag in Hα and 1.2-1.5·10^{-3} log(counts/s) in X-rays.

entire CCD to be read out in 1.5 s. Overhead in the computer operating system added up to one second to the total time required for each frame. The exposure times used in these observations were 5 ms, 10 ms, and 100 ms per image, giving duty cycles of approximately 10%, 20%, and 65%, respectively.

The long slit, with two windows defined, ensured that each image included a bright comparison star. The comparison star used is the photometric standard 35 of Henden & Honeycutt 1997 ($V = 13.498 \pm 0.001$, $B - V = 1.194 \pm 0.004$) situated $\sim 1'$ NNW of Cyg X-2. This star has been extensively monitored, and has shown no intrinsic variability down to 0.001 mag. Roughly half of the data was taken with a 3 nm FWHM filter centred on Hα and the remainder in white light (see Tab. 1). The seeing over three

nights ranged from 0.8 to 1.2 arcsec FWHM in Hα, and from 1.2 to 1.6 arcsec FWHM in white light.

Lightcurves were constructed for each observation sequence using square photometric apertures ranging in size from 1×1 to 11×11 pixels (0.4×0.4 to 4.4×4.4 arcsec). While the use of square photometric apertures, rather than circular apertures, is not conventional, there is little difference for apertures composed of a small number of pixels. For the larger apertures, there was no measurable difference in S/N when circular apertures were used, so for consistency, all photometric apertures used were square.

For each image the aperture is placed at the centroid of Cyg X-2, known to a fraction of a pixel. The comparison star aperture is placed at the (fixed) mean distance from Cyg X-2 to compensate for aperture losses. We checked that the PSFs of the two stars were similar and not affected by instrumen-

tal effects. Because every image includes both Cyg X-2 and the nearby comparison star, observed simultaneously under identical observing conditions, differential photometry allows the removal of temporal photometric throughput variations. We do not correct for extinction hence the broad band white light data can be subject to an airmass-correlated variation due to the colour difference between Cyg X-2 and the comparison star. However, since all our observations were done at airmass <1.2, with two-thirds of the data taken at airmass < 1.1, we feel this will have a negligible influence on the short timescale variability study.

We ignored images for which the centroiding algorithm had failed, a cosmic ray had been tagged inside the aperture, or (more commonly) those images in which the photometric aperture extended outside the unvignetted slit edges. The background in each window of each image was calculated as an average over the window, for pixels more than 10 pixels (4 arcsec) from the window center. We then computed the signal-to-noise ratio of the flux from Cyg X-2 as a function of aperture. The maximum S/N was obtained for an aperture of 7×7 pixels in white light and 3×3 pixels with the Hα filter. The comparison star data was extracted using the same aperture and the flux ratio computed to correct for lost flux and atmospheric variations. The final lightcurve is therefore the differential magnitude between Cyg X-2 and the comparison star. The S/N, chosen aperture, total number of measurements and number of measurements kept in each observation sequence can be found in Tab. 1.

The lightcurves, rebinned with 32 s resolution, are shown in Fig. 1. Note that 32 s is an elapsed time and that the actual exposure time and S/N in each bin varies with the observational setup. The 1σ error for each bin is obtained from the standard deviation of the averaged data points, hence implicitly assuming that the measurements are independent. Typical error values are given in column 4 of Tab. 2.

3   ANALYSIS AND RESULTS

3.1   X-ray data

To characterise the overall behaviour of Cyg X-2 in X-rays, a colour-intensity diagram was plotted using 32 s flux averages (Fig. 2). This diagram suggests that Cyg X-2 was on the normal branch during visits 1 and 2 (Aug 2), on the flaring branch during visit 3 (Aug 2) and on the horizontal branch during the visits of Aug 3 and 4. Power density spectra (PDS, see van der Klis 1989) were then constructed for each visit using all the detected photons. The high frequency (1 Hz–128 Hz) part of the PDS is the average PDS of 1 s long segments with a binsize of 1/256 s. The low frequency part ($\sim 10^{-4}$–0.5 Hz) is computed from a 1 s rebinned lightcurve. The PDS are normalised to units of r.m.s.^{2} Hz^{-1}, *i.e.,* fractional variance per unit frequency, and the expected Poisson measurement noise bias was subtracted. No corrections were made for background and PCA dead time, which are negligible.

The resulting PDS confirm that Cyg X-2 moved through the different branches of the Z track during the observations. On Aug 2, the absence of detectable broad band variability at frequencies above 1 Hz except for a weak QPO at
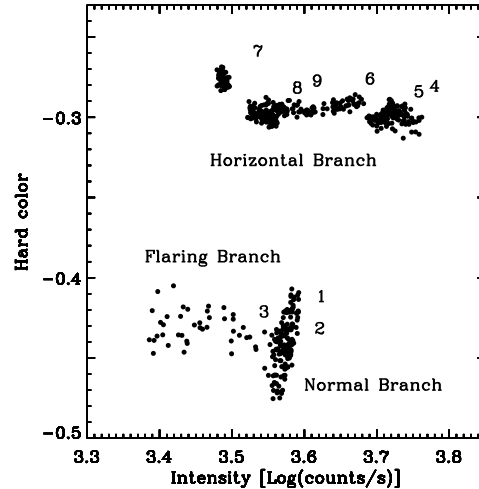

Figure 2. Hardness-intensity diagram of Cyg X-2 on Aug. 2, 3 and 4. The hard colour (y-axis) is the log of the count rate ratio between 5.7-9.8 and 2.0-5.7 keV (PCA channels 14-23 and 0-13). The intensity (x-axis) is from 2.0 to 9.8 keV. Each point is a 32 s average. The numbers indicate the position of the points from each X-ray visit (as labelled in Fig. 1).

6 ± 1 Hz during the second visit ($1.3\pm0.2\%$ r.m.s.) is typical of the normal/flaring branch. The Aug 3–4 PDS are typical of the horizontal branch with strong broad band variability peaking around 10 Hz and two QPOs varying between $\sim$24–34 Hz ($3.1\pm0.2\%$ to $4.4\pm0.2\%$ r.m.s.) and $\sim$50–63 Hz ($2.2\pm0.3\%$ to $2.3\pm0.3\%$ r.m.s.). In addition, low frequency variability is present in all the observations at frequencies below 0.1 Hz. These results are in line with previous, more extensive X-ray timing studies of this source (e.g. Wijnands et al. 1997; Kuulkers, Wijnands & van der Klis 1999; Wijnands & van der Klis 2001). We show in Fig. 3 some of the logarithmically rebinned X-ray PDS obtained on different nights.

3.2   Optical data

The 32 s binned optical lightcurves (Fig. 1) show variations above the measurement noise on timescales of minutes to hours. Quantitatively, the binned white light (resp. Hα) lightcurves have standard deviations of up to 0.04 mag (resp. 0.06) compared to the measurement noise of $\sim$ 0.003 mag (resp. 0.017; see §2.2). The values for each observation are in Tab. 2. Plotting the optical fluxes against the simultaneous X-ray fluxes, we find no obvious correlations between the two; but we note that the average white light flux was highest (by about 0.15 mag, second night), when the X-ray count rate was also highest (close to the vertex of the horizontal branch).

PDS were constructed for the optical data using a slight modification to the standard technique used for X-ray timing. For the optical data, we found the white noise level empirically instead of using Poisson statistics. The data were (fast) Fourier transformed and normalised by multiplying the amplitudes by $2/\mathrm{Var}(f)$, where $\mathrm{Var}(f)$ is total variance of the data f. This ensures the powers follow a χ^2_2 distribution when the lightcurve is dominated by (measurement)

white noise (*i.e.,* each point is independent and randomly taken from the initial flux distribution). The optical power spectra typically showed power at low frequencies and white noise at high frequencies. In these cases we divided by the average power at the frequencies where measurement noise dominates to recover the χ^2_2 statistics. The Fourier amplitudes give the fractional variance per frequency bin and, after subtraction of the constant white noise component, we plot the power $\times$ frequency in (dimensionless) units of r.m.s.^{2} to highlight the timescales with significant variability and ease comparison with the X-ray PDS (Fig. 3).

The low duty cycle of the data acquisition scheme introduces large amounts of spurious power in a Fourier transform covering several frames. To circumvent this problem, we separated the calculation of the power spectrum into two parts so that the transformed lightcurves had duty cycles close to 100%. At high frequencies, we computed a power spectrum of the images in each frame separately, then averaged the power spectra of all the frames. Since there are between 46 to 48 images (photometry points) in each frame with a time resolution of 5 ms (white light) to 100 ms (Hα), the resulting frequency range is about 5–100 Hz (white light) or 0.2–4.8 Hz (Hα), depending upon the observational setup (see Tab. 2). At lower frequencies we took the average flux of each frame (the sum of all images in a frame) and computed the power spectrum of the resulting lightcurve. The resulting frequency range is about 10^{-3}–0.05 Hz (see Tab. 2). The combined power spectrum is free of power leakage at the expense of a loss in frequency resolution and coverage. At high frequencies, the averaging of the individual spectra diminish the measured power from a highly coherent signal, because the contributions from each frame are not summed in-phase.

Significant power is present in all of the datasets at very low frequencies (below 3×10^{-3} Hz in white light and 10^{-3} Hz in Hα) except during the short August 3 Hα observation. The total r.m.s. of the flickering is estimated by integrating over the frequencies where power is detected above the 3σ single trial level. We obtain values of 1–3% r.m.s. (see Tab. 2) which are consistent with the standard deviation of the 32 s binned lightcurve. The optical variability is about an order of magnitude smaller than that seen in the X-ray lightcurves on the same frequency range.

At higher frequencies, statistically significant power is detected in the white light observation of Aug. 3, when Cyg X-2 was on the horizontal branch with a high X-ray flux. The total r.m.s. is about 1% (0.02–0.07 Hz). Unfortunately, this is the only detection of optical variability at high frequency in our limited dataset. Independent confirmation would be desirable. The very low frequency power in both optical and X-rays is reasonably approximated by $P_\nu \sim \nu^{-2}$ (*i.e.,* $\nu P_\nu \sim \nu^{-1}$ in Fig. 3). We obtained an upper limit to the flickering power in the cases where none was detected by calculating the total r.m.s. of power with this particular shape that would have yielded a 3σ detection (typically a few %, see Tab. 2). We also computed 3σ upper limits to the r.m.s. of a sinusoidal signal. Both of these upper limits take into account the number of trials in the frequency range. All of the results may be found in Tab. 2.

3.3 Cross-correlation

We cross-correlated each of the nine simultaneous X-ray and optical datasets (Tab. 1). The X-ray data, which have the highest time resolution, were corrected to the local Palomar time and rebinned in an identical way to the optical data set, yielding two continuous lightcurves with the same resolution ($\Delta t = 5$, 10 or 100ms). The cross-correlation function at a lag $k\Delta t$ is defined as (e.g. Edelson & Krolik 1988):

$$C(k\Delta t) = \frac{1}{M} \sum_{j-i=k} \frac{(o_i - \bar{o})(x_j - \bar{x})}{\sigma_X \sigma_{opt}}, \tag{1}$$

where o is the optical lightcurve, x the X-ray, the bar symbolises the average of the dataset and σ are the standard deviations. $C(k\Delta t)$ is an average over the M pairs of points which are $k\Delta t$ apart. The variance of the M averaged discrete correlations gives an estimate of the error on C. The above is efficiently computed in Fourier space for continuous lightcurves with the same Δt:

$$C(k\Delta t) = \frac{1}{\sigma_X \sigma_{opt}} \left\{ \frac{F^{-1}(F_o F_x^\star)}{F^{-1}(F_{w_o} F_{w_x}^\star)} \right\}_k, \tag{2}$$

where F is the (fast) Fourier transform, $\star$ is the conjugate and the w are window functions (a timeseries with value 1 when data are taken, 0 elsewhere).

There were no obvious trends on timescales $\gtrsim$10 min where the datasets are not long enough to clearly establish correlations. For the cross-correlations below 10 min, we subtracted piecewise linear fits in 600 s increments to the datasets to smooth out any underlying long timescale variation. The X-ray and optical data did not show any significant correlations down to 5 ms (100 ms). Cross-correlating with different energy selected X-ray lightcurves (2.0–5.7 keV, 5.7–9.8 keV, 9.8 keV and above) gave identical results.

4 DISCUSSION

Our dataset is consistent with previous studies reporting variations in the optical continuum of Cyg X-2 of $\sim$0.5 mag in days, $\sim$0.1 mag in hours and $\sim$0.05 mag in minutes (Kristian et al. 1967; Kruszewski et al. 1974; Kilyachlov 1978; Beskin et al. 1979). Orbital ellipsoidal modulation aside, there are few well-established features in the optical variability of Cyg X-2. There is a trend for the continuum to become bluer in *U-B* as Cyg X-2 becomes brighter (*B-V* staying $\sim$ constant; Lyutyi & Sunyaev 1976; Basko et al. 1976). Varying fluxes and FWHM on timescales $\gtrsim 1$ hr were also noticed early on in Hα, Hβ, HeII λ4686 and the Bowen blend (Johnson & Golson 1969; Cowley et al. 1979).

The evolution from the horizontal to the flaring branches in Cyg X-2 like sources has been proposed to reflect an increasing mass accretion rate in the disc (see discussion in Homan et al. 2002). This could be due to fluctuations in the mass transfer rate from the donor star or to fluctuations in the angular momentum transport processes, presumably on the disc viscous timescale. Interestingly, Hα is sometimes in absorption (Chuvaev 1976): in dwarf novae, the Balmer lines evolve from emission to absorption during the rise to outburst when the mass accretion rate increases (e.g. Szkody, Piché & Feinswog 1990). However, mass accretion rate changes are hard to reconcile with rapid (hours)

Table 2. Optical Variability of Cyg X-2

Date	Band	Δt ms	err* 10^{-3} mag	$\sigma^\star$ mag	ν_{min}-ν_{max} mHz	pulse % r.m.s.	total % r.m.s.	ν_{min}-ν_{max} Hz	pulse % r.m.s.	total % r.m.s.
Aug, 2	Hα	100	14	57	0.12-66	<0.4	3.4	0.21-5	<1.2	<2.5
Aug, 3	Hα	100	18	24	0.30-66	<0.7	<1.6	0.21-5	<1.9	<3.8
Aug, 4	Hα	100	16	37	0.07-66	<0.5	2.1	0.21-5	<1.4	<2.8
Aug, 2	wl	5	2.4	14	0.33-200	<0.2	1.0	4.35-100	<0.3	<0.6
Aug, 3	wl	10	2.0	41	0.07-160	<0.2	2.2	2.12-50	<0.3	1.1
Aug, 4	wl	5	2.6	14	0.28-160	<0.2	0.8	4.35-100	<0.4	<0.7

wl is white light; err* is the estimated error of a 32 s photometry bin (in mmag) and $\sigma^\star$ is the standard deviation of the 32 s binned lightcurve (in mmag; see Fig. 1); the optical variability is studied in two frequency ranges (see §3.2 for details): ν_{min}-ν_{max} give the corresponding frequency ranges; pulse gives the r.m.s. upper limit for a sine signal; total is the broad band r.m.s. variability or upper limit (assuming $F_\nu \propto \nu^{-2}$ coloured noise).
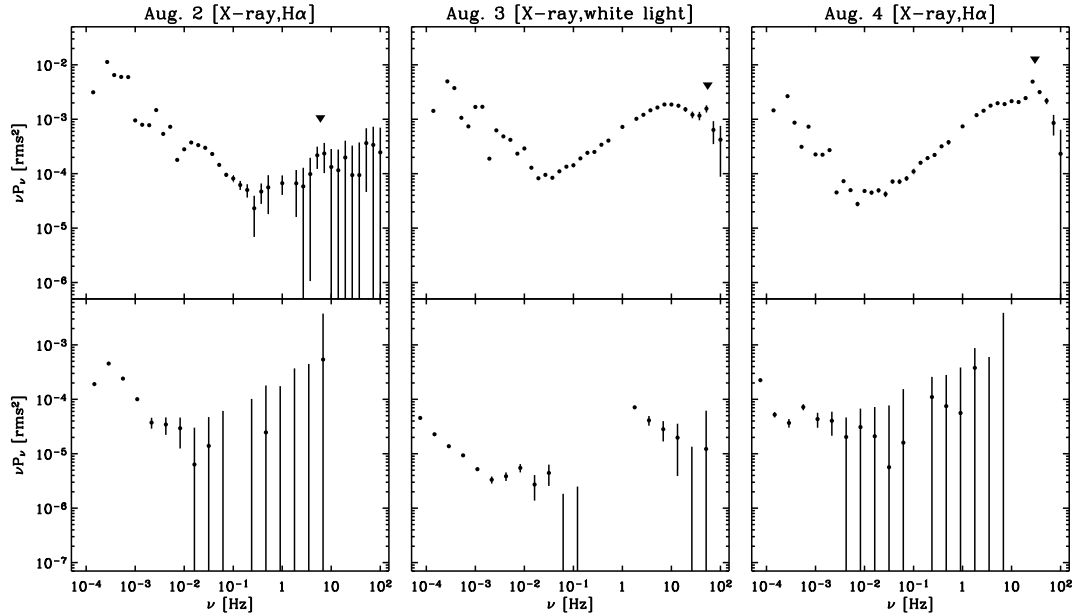

Figure 3. Temporal variability power spectra for the X-ray (top) and optical (bottom) data on different nights. White noise has been removed, the power normalised to units of r.m.s.^{2} Hz^{-1} and multiplied by frequency. The frequency range that contributes most to variability and its r.m.s. are thus easily identified. We also plot 3σ (single trial) error bars to help assess the statistical significance of the various features. The bottom of the first panel shows the power spectrum of the long Hα dataset taken on August 2; top shows the X-ray power spectrum from the simultaneous RXTE data (two visits, see Fig. 1). Second (resp. third) panel is for the long white light (resp. Hα) dataset taken on August 3 (resp. 4). The power spectra have been logarithmically rebinned. Downward arrows in the X-ray panels highlight the location of the QPOs discussed in §3.1.

variations changes unless they originate in the inner disc where the timescales are short.

Variations in the inner region can affect the optical output of the disc via non-local irradiation. The observed correlation between high ionisation line fluxes (HeII, CIII/NIII) and the optical continuum of Cyg X-2 does suggests that reprocessing plays a major role (Ilovaisky et al. 1979; van Paradijs et al. 1990; O'Brien 2001). Some of the long timescale X-ray fluctuations of Cyg X-2 have been argued to be due to varying obscuration, perhaps by an inner disc warp (Kuulkers & van der Klis 1995; Kuulkers, van der Klis & Vaughan 1996; Vrtilek et al. 1990,

2003). Changes in the albedo or geometry of reprocessing would lead to complex correlations between X-rays and optical (Esin, Lasota, & Hynes 2000). O'Brien (2001) found that the optical and X-ray fluxes were correlated on the horizontal branch, but anticorrelated on long timescales in the normal and flaring branches. Curiously, on shorter timescales (∼1 min), the X-ray and optical on the flaring branch were correlated. O'Brien proposed that several components with different intrinsic timescales contribute to the optical emission. Our observation of an order of magnitude lower variability in optical compared to X-rays on long timescales (§3.2) is consistent with reprocessing of a fraction

of the X-rays, but we did not find significant correlations to support this.

As argued in §1, variability and X-ray/optical correlations on short timescales could provide constraints on emission sites in Cyg X-2. Previous studies found no variability in the optical continuum below ~ 1 min (Chevalier et al. 1976; Auriemma et al. 1978; Ilovaisky et al. 1978). With a factor 2–5 better sensitivity and a longer dataset, we find some evidence for broad band variability at frequencies of few Hz in the continuum when Cyg X-2 was optically bright and on the horizontal branch; but we find no correlations with the X-ray noise component that peaks at ~ 10 Hz in this state. For rapid line variability, Canizares & McClintock (1975) give an upper limit of 8% to the pulsed fraction of the HeII flux between 0.1 and 125 Hz. We do not find variability in the Hα line on timescales shorter than 1 min.

In contrast with Cyg X-2, the other optically bright Z source, Sco X-1, shows correlated X-ray and optical flares on a 1–60 s timescale when it is on the flaring branch (Ilovaisky et al. 1980; Petro et al. 1981). The optical flares are 20 s filtered versions of the X-rays, probably as a result of non-local reprocessing. Similar behaviour is not seen in Cyg X-2, although the X-ray flux and variability are comparable. A different irradiation geometry, as mentioned in the previous paragraph, might explain their absence.

We did not find evidence for correlated X-ray – Hα variations due to solar-like flares. However, Hα emission could be powered by flares that are too weak to be detected individually and occurring at a fast enough rate that correlations are lost. For instance, Poutanen & Fabian (1999) discuss a model for the X-ray timing characteristics of Cyg X-1 in which the rapid variability is due to flare avalanches in the disc. Only rare large flares from the high luminosity end of the distribution function can be distinguished in the X-ray flux of Cyg X-1 (Gierliński & Zdziarski 2003).

Calculating the thin disc response to irradiation by high energy electrons produced in flares, Williams & Maletesta (2002) find that an avalanche model can explain the Hβ emission and the optical continuum flickering observed in cataclysmic variables (which have accretion discs comparable to those in LMXBs). Only 4% of the flare energy is used to produce the variable V band flux. A similar model might apply to Cyg X-2 with, perhaps, more of the flare energy deposited in the disc to take into account the higher optical/X-ray flux ratio. The high number of active regions required is likely to have a significant impact on the X-ray spectral properties (*e.g.,* di Matteo, Celotti & Fabian 1999). X-ray emission by bremsstrahlung or Compton upscattering is not modelled by Williams & Maletesta (2002). If flares give rise to the broad band X-ray noise (with r.m.s. levels of a few %) then our upper limit of $\sim 3\%$ r.m.s is too high to detect their Hα signature.

5   CONCLUSION

We obtained Hα or white light lightcurves of Cyg X-2 with high time resolution simultaneously with X-ray data. Two (mutually non exclusive) mechanisms may link the two wave bands: non-local reprocessing of X-ray photons emitted close to the compact object or local reprocessing of particles accelerated in magnetic flares. We find broad band variability on timescales longer than a minute and some evidence on sub-second timescales in one white light observation. No correlations are found. Our observations cannot be used to distinguish between non-local or local reprocessing. The lack of correlations could be explained either by unfavourable irradiation circumstances (non-local case) or because large, identifiable magnetic flares are scarce (local case).

The prospects offered by rapid optical photometry have proven difficult to fulfill. Part of the difficulty lays in assembling a large, coherent, simultaneous X-ray and optical dataset with secure calibrations from which trends can emerge (*i.e.,* the strategy behind the success of X-ray timing studies). More problematic are the small amplitude of the expected variability and limited number of bright enough objects for which sensitive enough observations and comparisons can be made. In principle, the present generation of 8–10 m class telescopes could remedy that.

REFERENCES

Auriemma G., Giovannelli F., Ranieri M., 1978, A&A, 69, 391

Balbus S. A., Hawley J. F., 1998, Rev. Mod. Phys., 70, 1

Basko M. M., Goranskii V. P., Lyutyi V. M., Ruzan L. L., Sunyaev R. A., Shugarov S. Yu., 1976, Soviet Astron. Let, 2, 214

Beskin G. M., Neizvestnyi S. I., Pimonov A. A., Plakhotnichenko V. L., Shvartsman V. F., 1979, Soviet Astron. Let, 5, 271

Canizares C. R., McClintock J. E., 1975, ApJ, 200, 177

Chevalier C., Bonazzola S., Ilovaisky S. A., 1976, A&A, 53, 313

Chuvaev K. K., 1976, Soviet Astron. Let, 2, 211

Cowley A. P., Crampton D., Hutchings J. B., 1979, ApJ, 231, 539

Done C., 2002, Phil. Trans. of the Royal Society (Series A), 360, 1967

di Matteo T., Celotti A., Fabian A. C., 1997, MNRAS, 291, 805

di Matteo T., Celotti A., Fabian A. C., 1999, MNRAS, 304, 809

Dulk G. A., 1985, *Solar Radiophysics*, Cambrige University Press: Cambridge

Edelson R. A., Krolik J. H., 1988, ApJ, 333, 646

Esin A. A., Lasota J.-P., Hynes R. I., 2000, A&A, 354, 987

Fabian A. C., Guilbert P. W., Motch C., Ricketts M., Ilovaisky S. A., Chevalier C. 1982, A&A, 111, L9

Galeev A. A., Rosner R., Vaiana G. S., 1979, ApJ, 229, 318

Gierliński M., Zdziarski A. A., 2003, MNRAS, 343, L84

Haardt F., Maraschi L., 1991, ApJ, 380, L51

Hasinger G., van der Klis M., 1989, A&A, 225, 79

Henden A. A., Honeycutt R. K., 1997, PASP, 109, 441

Homan J., van der Klis M., Jonker P. G., Wijnands R., Kuulkers E., Méndez M., Lewin W. H. G., 2002, ApJ, 568, 268

Hynes R. I. et al. 2003a, MNRAS, in press (astro-ph/0306626)

Hynes R. I., Charles P. A., Casares J., Haswell C. A., Zurita C., Shahbaz T., 2003b, MNRAS, 340, 447

Ilovaisky S. A., Chevalier C., Chevreton M., Bonazzola S., 1978, A&A, 67, 287

Ilovaisky S. A., Chevalier C., Motch C., Janot-Pacheco E., Branduardi G., Mason K. O., White N. E., Sanford P. W., 1979, IAUC, 3325

Ilovaisky S. A., Chevalier C., White N. E., Mason K. O., Sanford P. W., Delvaille J. P., Schnopper H. W., 1980, MNRAS, 191, 81

Johnson H. M., Golson J. C., 1969, ApJ, 155, L91

Kanbach G., Straubmeier C., Spruit, H. C., Belloni T. 2001, Nature, 414, 180

Kristian J., Sandage A., Westphal J. A., 1967,ApJ, 150, L99

Kuulkers E., van der Klis M., 1995, A&A, 303, 801

Kuulkers E., van der Klis M., Vaughan B. A, 1996, A&A, 311, 197

Kuulker E., Wijnands R., van der Klis M., 1999, MNRAS, 308, 485

Kruszewski A., Semeniuk I., Schwarzenberg-Czerny A., 1974, Inf. Bull. Var. Stars, No. 933

Kilyachkov N. N., 1978, Soviet Astron. Let, 4, 217

Leahy D. A. et al., 1983, ApJ, 266, 160

Lyutyi V. M., Sunyaev R. A., 1976, Soviet Astr, 20, 290

McGowan K. E., Charles P. A., O'Donoghue D., Smale A. P., 2003, MNRAS, submitted (astro-ph/0307373)

Motch C., Ricketts M. J., Page C. G., Ilovaisky S. A., Chevalier C. 1983, A&A, 119, 171

Mumford G. S., 1970, in Proc. IAU Symp. 37 *Non-Solar X-and Gamma-Ray Astronomy*, Gratton L. (Ed.), Kluwer, Dordrecht, p. 177

Orosz J. A, Kuulkers E., 1999, MNRAS, 305, 132

O'Brien K., 2001, proceedings of the first Galway workshop on high time resolution astrophysics, Galway, ASP conference series (astro-ph/0110267)

O'Brien K., Horne K., Hynes R. I., Chen W., Haswell C. A., Still M. D., 2002, MNRAS, 334, 4

Petro L. D., Bradt H. V., Kelley R. L., Horne K., Gomer R. 1981, ApJ, 251, L7

Poutanen J., Fabian A. C., 1999, MNRAS, 306, L31

Shakura N. I., Sunyaev R. A., 1973, A&A, 24, 337

Swank J. H., Jahoda K., Zhang W. , Giles A. B., 1996, in *The Lives of Neutron Stars"*, Alpar M. A., Kiziloglu U., van Paradijs J. (eds.), NASO ASI Ser C., 450, (Boston: Kluwer), 525

Szkody P., Piché F., Feinswog L. 1990, ApJS, 73, 441

van der Klis M., 1989, in *Timing Neutron Stars*, Ogelman H., van den Heuvel E. P. J. (eds), NATO ASI Series C, 262, 27 (Kluwer, Dordrecht)

van der Klis M., 2000, ARA&A, 38, 717

van Paradijs J., Allington-Smith J., Callanan P., Charles P. A., Hassall B. J. M., Machin G., Mason K. O., Naylor T., Smale A. P., 1990, A&A, 235, 156

van Paradijs J., McClintock J. E., 1995, in X-ray Binaries, (Cambridge: Cambridge University Press), Chap. 2

Vrtilek S. D., Raymond J. C., Boroson B., McCray R.,

Smale A., Kallman T., Nagase F., 2003, PASP, in press, (astro-ph/0305459)

Vrtilek S. D., Raymond J. C., Garcia M. R., Verbunt F., Hasinger G., Kürster M., A&A, 2002, 235, 162

Wijnands R., van der Klis M., Kuulkers E., Asai K., Hasinger G., 1997, A&A, 323, 399

Wijnands R., van der Klis M., 2001, MNRAS, 321, 537

Williams G., Maletesta K., 2002, AJ, 123, 1095